

Features of Capacitance and Mobility of Injected Carriers in Organic Layers Measured by Impedance Spectroscopy

José M. Montero^[a, b] and Juan Bisquert^{*[a]}

Abstract: Transport of charge carriers in organic layers plays a relevant role in the performance of electronic devices such as light-emitting diodes, solar cells, and photodetectors. The presence of energetically distributed traps severely affects the measured transport coefficient and the charge-storage features in the film. We summarize recent theoretical work on impedance spectroscopy models for space-charge limited current of a single carrier in a multiple trapping model, which describes the experimental behavior usually

observed in organic layers with injected charge carriers well. Two main physical effects are obtained from the numerical and analytical treatment. First, carriers in slow traps that do not follow alternating current modulation provide an increase in the capacitance at low frequency, and second, those in fast traps remain in equilibrium with the transport state increasing the transit time. Analysis also provides a unified interpretation of models with field- or carrier-density dependence on mobility.

Keywords: capacitance · charge carrier injection · electron transfer · impedance spectroscopy · mobility · transport in organic materials

1. Introduction

In recent times, electronic devices based on light-emitting diodes (LEDs) have triggered increasing widespread application of the so-called LED technology for displaying information (e.g., light indicators and panel displays) or even for a promising low-cost general illumination.^[1] Particularly, Western countries are currently phasing out light bulbs due to energetic needs.^[2] The appearance and ongoing development of complementary or alternative organic light-emitting diodes (OLEDs) has attracted global research interest to achieve low-consumption devices.^[3–6] OLED technology represents a promising light source for general space illumination, since white OLEDs have already reached a value of 90 lumens per watt (lm W^{-1}), surpassing the benchmark of fluorescent tube efficiency ($60\text{--}70 \text{ lm W}^{-1}$).^[7] Low-cost manufacturing processability, large areas, and flexible displays with good quality of vision independent of the angle may be achieved.^[8]

The performance of organic electronic devices strongly depends on the physical processes taking place either at the metal–organic interface (i.e., injection) or in the bulk semiconductor (i.e., transport and recombination).^[9–16] The latter phenomena are closely related to charge-transport mobility in disordered organic materials, which is actually the crucial parameter governing device operation.^[17] Moreover, transport in organic layers, driven by space-charge limited current (SCLC),^[18–21] requires an additional interpretation of mobility by different semiempirical models with field or density dependence.^[22–25]

From an experimental point of view, the measurement of mobility is commonly performed through the study of

transit times (i.e., the time needed for carriers to cross a sandwiched sample from electrode to electrode) in a wide range of methods available in the literature: time-of-flight, transient electroluminescence, dark injection, and impedance spectroscopy (IS) among others.^[26–30]

IS has been used in the analysis of organic and hybrid devices, such as dye-sensitized solar cells (DSSCs) and organic solar cells.^[31] There are several advantages to this technique for the determination of device parameters and characteristics. (i) It is a small perturbation and noninvasive method that can be applied under any operating conditions and thicknesses of the device, so that the dependence of parameters on voltage, for example, can be scanned. (ii) It allows for the simultaneous determination of several characteristics, such as capacitance and transport resistance. This allows the carrier distribution in the device to be probed at the same time as kinetic information about carrier displacement is obtained.^[31–34]

In the case of single-carrier transport in which SCLC predominates, traditional IS theory shows a simple corre-

[a] J. M. Montero, J. Bisquert
Photovoltaics and Optoelectronic Devices Group
Departament de Física
Universitat Jaume I
12071 Castelló (Spain)
e-mail: bisquert@fca.uji.es

[b] J. M. Montero
Gymnázium Hladnov
Hladnovska 35
71000 Ostrava (Czech Republic)

lation of the capacitance step (as a function of frequency) with a step in the conductance that allows the transit time to be extracted. In reality, however, IS measurements in organic transport layers show much more complex characteristics,^[23,35,36] especially due to the energetic disorder of the localized states in the band gap (traps).^[37–46] Recently, a series of works have reported simulation and interpretation of the influence of traps in the IS response of organic layers.^[39, 47–50] It was also shown that a trapped-controlled transport, based on SCLC multiple trapping affected by an exponential distribution of traps, was able to explain the interconnection between the field- and density-dependent mobility models.^[48,49] In addition, the measurements of capacitance spectra from IS, especially at low frequencies, were reproduced by this trap-controlled transport framework.^[39,48,49] This review provides a summary of these findings, with an emphasis on the interpretation of the observed capacitance spectra in terms of the behavior of traps, as a tool for the physical understanding of transport and capacitance in organic layers.

2. Traditional Transport Models

In the 1990s, the field-dependent mobility model was initially proposed by Bässler, as the result of assuming hopping transport in a Gaussian density of states (DOS).^[51,52] ■■Bässler not an author of ref. [52], please check■■■ Random walk with Monte Carlo simulations yielded the well-known Poole–Frenkel expression [Eq. (1)]:

$$\mu(E) = \mu_0 \exp(\gamma\sqrt{F}) \quad (1)$$

in which μ_0 is the zero-field mobility for a particular carrier species in the material, F is the electric field, and γ is a temperature-dependent material constant. These parameters are closely related to the degree of disorder. The field-dependent mobility description in sandwiched organic films, composed of either conducting polymers (e.g., poly(*p*-phenylene vinylene) (PPV) derivatives) or small-molecule organic semiconductor (e.g., tris(8-hydroxyquinolate)aluminum (Alq3)), became widely accepted.^[53–55] The experimental steady-state response of organic layers, given by current–density voltage characteristics ($J - V$), was treated in terms of a manageable approximation proposed by Murgatroyd [Eq. (2)]:^[56,57] ■■Murgatroyd not an author of ref. [57], please check■■■

$$J \approx \frac{9}{8} \frac{\epsilon\mu_0}{L^3} V^2 \exp(0.89\gamma\sqrt{V/L}) \quad (2)$$

in which L is the sample thickness and V is the voltage drop in the bulk layer in SCLC. Fittings to Equation (2) were carried out to extract mobility parameters in different materials.^[58–60]

However, the accepted interpretative framework changed due to breakthrough studies on charge transport in field-effect transistors. Tanase et al. pioneered a comparison of mobility values for two solution-processed organic polymers, OC₁C₁₀-PPV and poly(3-hexylthiophene) ■■■ok?■■■ (P3HT), performed in two different configurations, namely, field-effect transistors and hole-only diodes.^[53,61] The former structure displayed mobility results up to three orders of magnitude higher than the latter configuration. This experimental fact endorsed the density-dependent mobility model proposed by Vissenberg and Matters in amorphous organic transistors, which stems from hopping percolation in an exponential DOS.^[62] Thus, the density-dependent mobility is given by Equation (3):

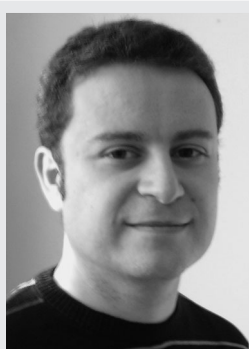
$$\mu(n) = an^b \quad (3)$$

in which a and b are model constants and b is given by Equation (4):

$$b = \frac{T_t}{T} - 1 \quad (4)$$

which is a coefficient that relates the operating temperature T to the characteristic trap temperature of the exponential distribution T_t . As demonstrated by Arkhipov et al., hopping transport in disordered materials can be reduced to a trap-controlled transport composed of an effective transport level and a broad distribution of local-

José M. Montero received his bachelor's degree in physics from Universidad de Salamanca in 2004 and his Ph.D. from Universitat Jaume I of Castellón in 2010 with support from the FPI program. His major research topic comprises studies on organic optoelectronics such as modeling charge transport in organic materials by means of impedance spectroscopy.



Juan Bisquert is a professor of applied physics at Universitat Jaume I de Castelló (<http://www.elp.uji.es/jb.php>). He conducts experimental and theoretical research on nanoscale devices for the production and storage of clean energies. His main topics of interest are dye- and quantum-dot-sensitized solar cells, organic solar cells, and solar fuel production.



ized states (traps) that only retain mobile charges.^[63] The experimental steady-state response of organic layers, given by current–density voltage characteristics ($J - V$), was analyzed in terms of Equation (5):^[64]

$$J = e\mu_0 N_c \left(\frac{\varepsilon}{eN_t}\right)^l \left(\frac{l}{l+1}\right)^l \left(\frac{2l+1}{l+1}\right)^{l+1} \frac{V^{l+1}}{L^{2l+1}} \quad (5)$$

$$l = \frac{T_t}{T} \quad (6)$$

in which e is the elementary charge, l is given by Equation (6), N_c is the effective density of states in the extended state, and N_t is the trap effective density of states. Mobility values have been obtained by fitting current–potential curves to Equation (5).^[65]

Currently, several authors are considering this framework based on transport through an extended state under the influence of an exponential density of traps.^[50, 66–68] In forthcoming sections, we summarize the main results of this multiple trapping approach in SCLC studied in detail in three previous works.^[39, 47–50]

3. Trap-Controlled Transport Model

The description of trapping–diffusion transport, typically considered in electronic devices such as DSSCs, depicts a homogeneous system that can be analytically solved.^[69–72] However, trapping–drift transport of charge carriers, commonly observed in single-carrier diodes and OLEDs, entails a highly inhomogeneous configuration along the device thickness that requires numerical solutions. This trap-controlled transport, solved by computational simulations, comprises four major assumptions in the model implementation: (1) ohmic contacts, (2) SCLC, (3) an intrinsic trap-free constant mobility μ_{0n} , and (4) trapping–detrapping kinetics of an exponential distribution of traps in the band gap.

Figure 1 shows the configuration of the single-carrier device. Efficient charge injection of carriers from the metallic contacts occurs, since metal work functions are close enough to the transport level and can supply as many carriers as the material is capable to transport. Therefore, the so-called bulk-limited regime governs the performance of the electron-only device instead of the injection-limited one.^[9, 73] Charge carriers drift by the local electric field from the injecting electrode to the collecting contact (i.e., SCLC) under the influence of trapping–detrapping kinetics of the exponentially localized states that only retain mobile carriers.^[48] The interplay between transport and trapping processes occurring at once critically determines the electronic characterization of the organic material as described in the following sections.

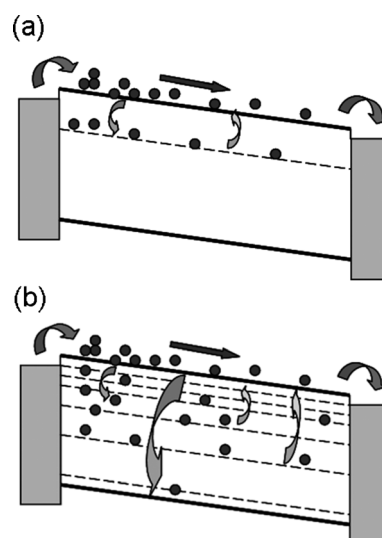


Figure 1. Schematic energy band diagram of an electron-only device (a) with a single-trap level and (b) with an exponential density of traps. Red arrows represent interfacial transport, namely, injection and extraction; the blue arrow is the bulk transport; and orange and green arrows are the trapping and release kinetics, respectively.

3.1. Steady-State Characteristics

Experimental measurements of $J - V$ curves are usually analyzed to interpret the performance behavior and charge transport of a wide range of electronic devices, such as OLEDs,^[74, 75] thin-film transistors (TFT),^[61] and solar cells (PV).^[76] In single-carrier organic layers, ordinary experimental data displayed a current density dependent on voltage higher than the well-known Mott–Gurney square law $J \propto V^2$.^[77] Thus, the field-dependent mobility model [Eq. (2)] was initially applied to properly analyze the results. Later, the density-dependent picture [Eq. (5)] dominated the interpretations to explain the extra current required along the voltage range. Simulations of the trap-controlled transport model (Figure 2) support this framework for a certain voltage domain because most of the ohmically injected carriers are mainly located in trapping states ($n_t \gg n_c$). However, at higher voltages the traps are filled, all additional injected carriers drift by the transport state ($n_t \ll n_c$), and the transport model predicts the Mott–Gurney square law modified by shallow-trap contribution [Eq. (7)]:^[49, 78]

$$J = \frac{9}{8} \varepsilon \theta \mu_{0n} \frac{V^2}{L^3} \quad (7)$$

in which $\theta^{-1} (= 1 + \langle n_t \rangle / \langle n_c \rangle)$ is a carrier density dependent factor of trapped n_t and free charge n_c located by the shallow traps.^[79]

Figure 3(a) illustrates the inhomogeneous distribution we are dealing with by displaying the Fermi level along the device thickness at 3 V. In the vicinity of the injecting

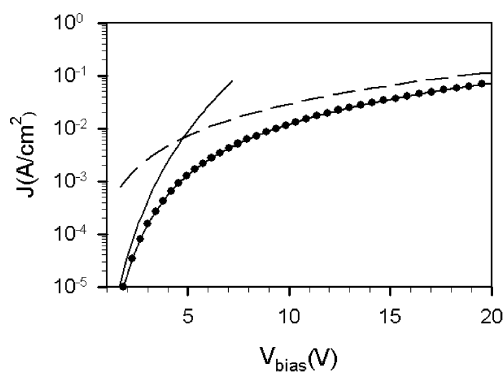


Figure 2. Simulations of current density–voltage characteristics (line and scatter plot)

contact, the functional shape is especially abrupt with a smoother functional dependence in the wide range of the thickness. In other words, many carriers build up by the injecting region meanwhile the rest of the carrier density distribution becomes rather uniform. Therefore, the assumption of an average Fermi level (E_F) makes sense and simplifies the SCLC multiple-trapping interpretation. Under this consideration, Figure 3(b) shows the occupied density of traps in energy, the empty ones, and the occupancy.

3.2. Impedance Response

Experimental measurements of capacitance spectra extracted from IS are considered a powerful tool to describe transport properties in electronic devices such as DSSCs and OLEDs.^[37,46,80,81] Charge-carrier mobility and energetic disorder in the band gap (i.e., localized states or traps) can be characterized in organic layers. The IS technique consists of the application of a small alternating current (ac) harmonic perturbation $v_{ac} = v_0 \cos(\omega t)$ over a direct current (dc) steady state of the device operation. Complex impedance, $Z(\omega) = v_{ac}(\omega)/i_{ac}(\omega)$, can be measured by means of the ac induced current, i_{ac} . However, the admittance, $Y(\omega)$, which is the inverse of the impedance, provides the electrical response of the system in terms of a resistor in parallel with a capacitor [Figure 4 and Eq. (8)].^[82–85]

$$Y(\omega) = i_{ac}/v_{ac} = g(\omega) + i\omega C'(\omega) \quad (8)$$

in which $\omega = 2\pi f$ is the linear frequency, $g(\omega)$ is the conductance, and $C'(\omega)$ is the dynamic capacitance. The representation of capacitance in the frequency domain, given by Equation (9), yields to the capacitance spectra commonly studied in experiments.^[15, 28, 42, 86–88]

$$C'(\omega) = \text{Re} \left[\frac{1}{i\omega Z(\omega)} \right] \quad (9)$$

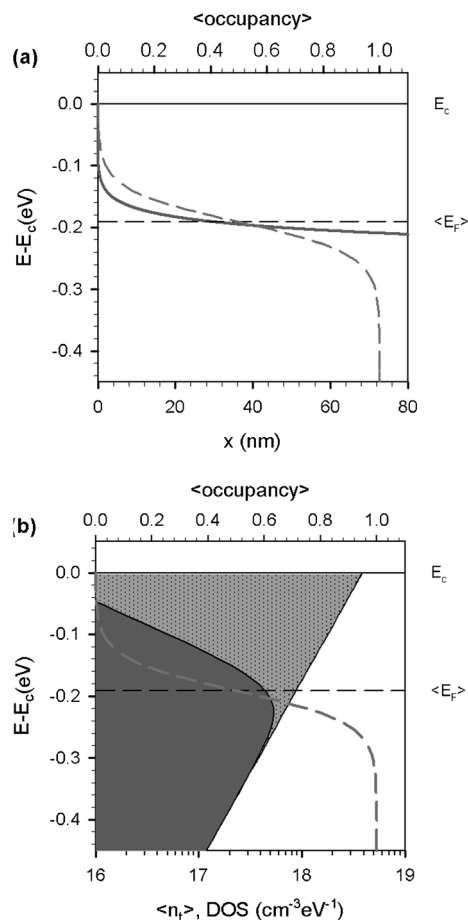


Figure 3. (a) Simulations at 3 V of the Fermi level along the thickness (solid line) and average occupancy (dashed line) stemming from the average Fermi level $\langle E_F \rangle$. (b) Colored area is displayed for the average occupied trap density of states (DOS), whereas the shaded area corresponds to the empty trapping density of states. Average occupancy is also printed (pink dashed line) together with average Fermi level $\langle E_F \rangle$ and transport energy level E_c as references.

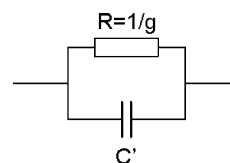


Figure 4. Equivalent circuit of bulk transport in an organic layer defined by IS.

As demonstrated in the literature, there is a strong correlation between the nature of traps lying in the band gap and the shape of the capacitance spectra.^[38,41,47] First, we summarize model results of capacitance by analyzing simulations of a single-trap level. Second, we extend these ideas from a single to an exponential density of localized states in the band gap to characterize experimental data.

3.2.1. Single-Trap Capacitance

The physical interpretation of this situation (Figure 5) is given in terms of two time processes occurring at once: transport and trapping–detrapping kinetics. The time needed for the carriers to cross the sample from electrode to electrode is the so-called transit time τ meanwhile trapping time τ_{trap} is defined by the intrinsic kinetics of traps. A classification of single shallow traps can be established, depending on which phenomenon dominates in the time domain, that is, which one is faster. Further details can be found in Ref.^[47] in terms of the capture coefficient c , which is the crucial parameter governing the trapping activity and stems from the nature of the trap.

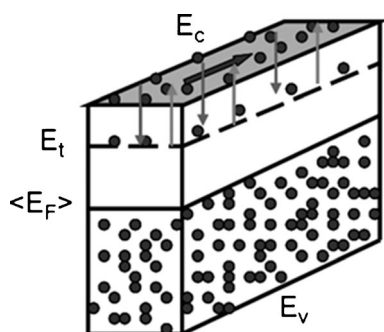


Figure 5. Schematic representation of an organic system composed of a transport level E_c (blue arrow) and a single shallow trap that traps and releases carriers (orange and green arrows, respectively). Below the average Fermi level, $\langle E_F \rangle$, full occupation is expected.

Figure 6 represents two different capacitance spectra (i.e., for a slow-shallow trap $\tau < \tau_{\text{trap}}$ and a fast-shallow trap $\tau > \tau_{\text{trap}}$) in comparison with the trap-free configuration. For a slow shallow trap, a low-frequency capacitance increase is observed, whereas there is no shift for a fast shallow one. However, a shift of the capacitance step-up occurs for the fast shallow trap and not for the slow shallow one. Let us explain both physical behaviors.

Low-frequency capacitance increase occurs when the trapped charge is not able to achieve a quasi-equilibrium with the carrier concentration in the transport level, that is, trapping kinetics cannot follow the small ac voltage signal. Therefore, this effect is characteristic of a slow shallow trap, as shown in Figure 7. The trapping time is larger than the transit one; this ensures that transport becomes the dominant process, that is, the fastest one. Capacitance step-ups define transit times and for slow shallow traps, no difference is observed compared with the trap-free spectrum.

The trap-limited mobility effect occurs when trapping kinetics are fast enough to follow the small ac voltage perturbation and the trapped charge can achieve quasi-equilibrium with the free charges in the transport level.

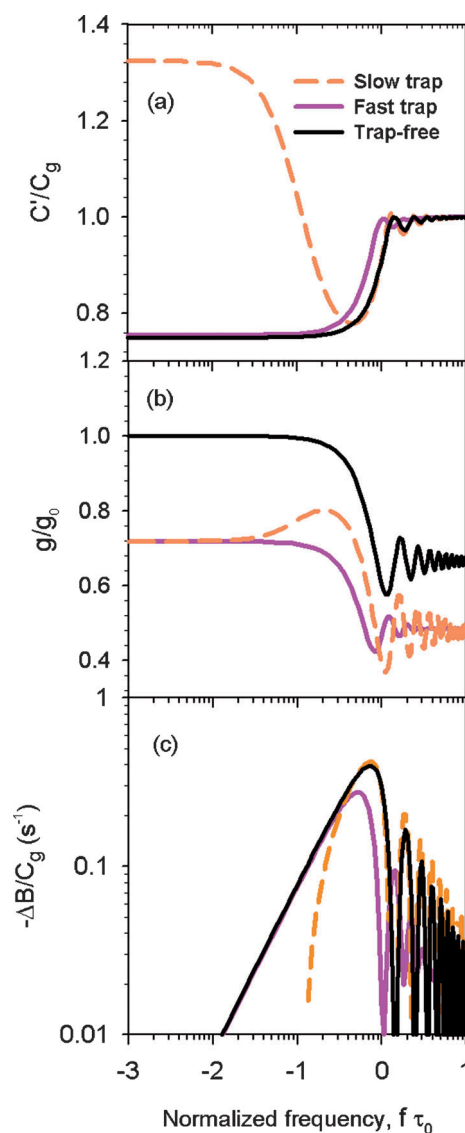


Figure 6. Simulation spectra for shallow traps at 2 V for (a) capacitance, (b) conductance, and (c) differential susceptance. Fast traps are plotted as pink lines, slow traps as orange dashed lines, and the trap-free spectrum is shown in black, as a reference. The frequency is normalized to the trap-free transit time, $\tau_0 = \frac{4L^2}{3\mu_0 V}$. (a) Capacitance spectra normalized to C_g for fast and slow traps. A low-frequency increase is displayed for slow traps, whereas it is not for the fast ones. (b) Conductance spectra normalized to g_0 for fast and slow traps start for low frequencies at $\theta \approx 0.71$ instead of at 1, as in the trap-free spectrum. For high frequencies, $2\theta/3$ is reached. (c) Negative differential susceptance $-\Delta B(\omega)$ normalized to C_g to extract transit times. In the case of fast trapping, the ac transit time is $\tau_{\text{ac}} = 1.36\tau_0$ ($\tau_0 = 221.6 \mu\text{s}$) with $\theta^{-1} \approx 1.40$, whereas for slow trapping no deviation from the trap-free value is presented.

Therefore, this feature is characteristic of a fast shallow trap, as shown in Figure 8. Every capacitance spectrum makes an upward step from 0.75 to 1 at a certain frequency. It defines transit times that can be determined by peaks of susceptance $-\Delta B(\omega)$. The shift of the capacitance step-ups is closely related to a deviation of transit

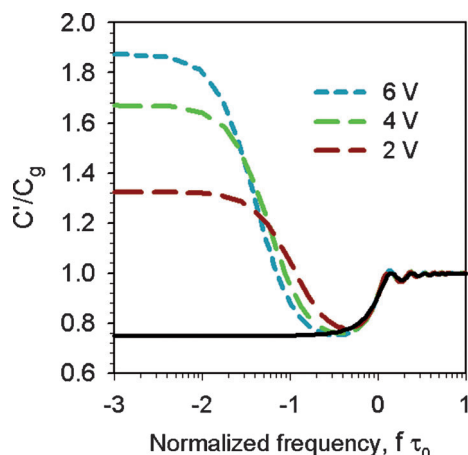


Figure 7. Model representations of capacitance spectra for slow shallow traps at 6, 4, and 2 V (from top to bottom). The trap-free spectrum is shown in black as a guide to the eye.

times, τ , and thus, to mobility, μ , as given by Equation (10):^[89]

$$\tau = \frac{4 L^2}{3 \mu V} \quad (10)$$

The trapping time is smaller than the transit one; this ensures that trapping kinetics becomes the dominant process, that is, the fastest one. Carrier transport from electrode to electrode is constantly altered by the action of fast trapping, causing a delay in transit time, that is, mobility reduction. The mobility dependence on voltage, found in IS experiments, can be interpreted in terms of trap-limited mobility.

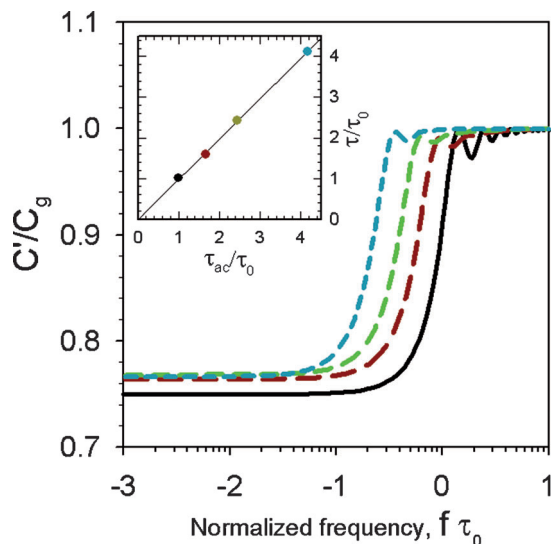


Figure 8. Simulated capacitance spectra steps for fast shallow traps at 6 V ($\tau_0 = 73.8 \mu\text{s}$) by varying the trap densities, from left to right: $N_t = 8 \times 10^{17}, 4 \times 10^{17}, 2 \times 10^{17}, 0 \text{ cm}^{-3}$. Upper-left panel shows an identification of transit times between the model and ac calculations.

Beyond this rather simple approach of SCLC transport of two levels, we extend this analysis to a broad distribution of localized states: an exponential distribution in the band gap. By detailed balance arguments, the detrapping time becomes larger the deeper is the trap. Hence, in the exponential distribution all types of traps are expected to be present.

3.2.2. Exponential-Trap Capacitance

The physical scheme of this configuration (Figure 9) consists of a transport state affected by a wide span of traps located by the energetic band gap. Further details can be found in Ref.^[48]. Both slow and fast shallow traps are present in the distribution, depending on the energy depth. Trapping–detrapping kinetics intersects carrier transport and both trapping effects occur, that is, low-frequency capacitance increase and trap-limited mobility. Fast shallow traps are those close to the extended state E_c and the lowest energy level E_L acting as purely fast can be expressed by Equation (11):

$$E_L = k_B T \ln \left[\left(\frac{3\pi\mu_0 V}{c N_c L^2} \right) \exp \left[\frac{(E_c - \langle E_F \rangle)}{k_B T} \right] - 1 \right] + \langle E_F \rangle \quad (11)$$

in which E_L is the limiting level that accounts for trapping activity, $\langle E_F \rangle$ is the average steady-state Fermi level, and E_c is the transport state. Traps below $\langle E_F \rangle$ are mainly occupied, whereas those above are mainly empty. Figure 10 shows a constant capture rate along the band gap, while the emission rate decreases. Active trap levels, E_t , behave as fast ones in the energy region of $E_c \geq E_t \geq E_L$ causing the trap-limited mobility effect. However, in the energy region of $E_L > E_t > \langle E_F \rangle$ trapping activity starts to gradually change from fast to slow kinetics, which critically re-

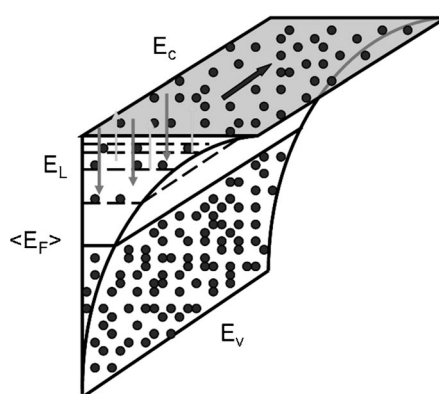


Figure 9. Schematic energy levels of the trap-controlled transport model. Transport in the extended state (blue arrow) affected by trapping and release kinetics (orange and green arrows) with fast trapping between E_c and E_L . Below the average Fermi level $\langle E_F \rangle$ full occupancy is expected and between E_L and $\langle E_F \rangle$ slow trapping action occurs.

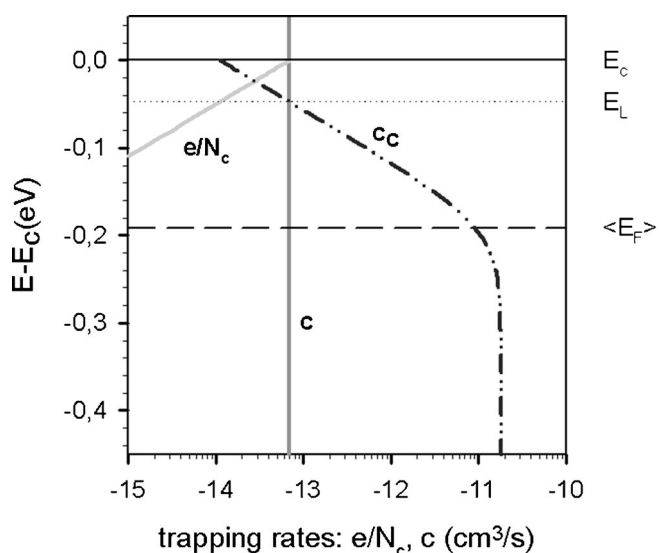


Figure 10. Trapping coefficients are displayed for the 3 V model simulation: normalized emission (e/N_c) and trapping (c) rates are represented by colored solid lines. The critical capture coefficient is given by a dash-dotted line. Reference energy levels are transport, E_c ; limit, E_L ; and average Fermi, $\langle E_F \rangle$, levels.

sults in the low-frequency capacitance effect of the capacitance spectra.

4. Experimental Behavior of Capacitance and Conductance

To compare the trap-controlled transport model with the experimental data, a series resistance, due to the metallic contacts, is added to the equivalent circuit shown in Figure 4 for computer calculations. The series resistance is responsible for an abrupt cutoff at high frequencies in the capacitance spectra. Model simulations carried out on a thin-film organic layer at different voltages (Figure 11) can be interpreted in terms of Equation (11) and results shown in Figure 10. At lower voltages, the average Fermi level $\langle E_F \rangle$ lies low in the band gap along with the limit level, E_L , but the relative position between them must always remain $E_L > \langle E_F \rangle$. As a consequence, fast shallow traps belonging to the energy region $E_c \geq E_t \geq E_L$ result in a noticeable trap-limited mobility effect. In addition, slow shallow traps located by the energy interval $E_L > E_t > \langle E_F \rangle$ produce a strong low-frequency capacitance increase. However, by increasing the applied voltage, $\langle E_F \rangle$ moves up, covering more localized states of the exponential density in the band gap and E_L moves up as well. Therefore, reduced low-frequency capacitance increase and less trap-limited mobility is expected as more voltage is applied to the bulk material.

Experimental capacitance spectra have been recently reported that show capacitance increase at low frequencies.^[23, 39, 42, 85, 90–94] This behavior has sometimes been interpreted in terms of a frequency-dependent mobility.^[35,36]

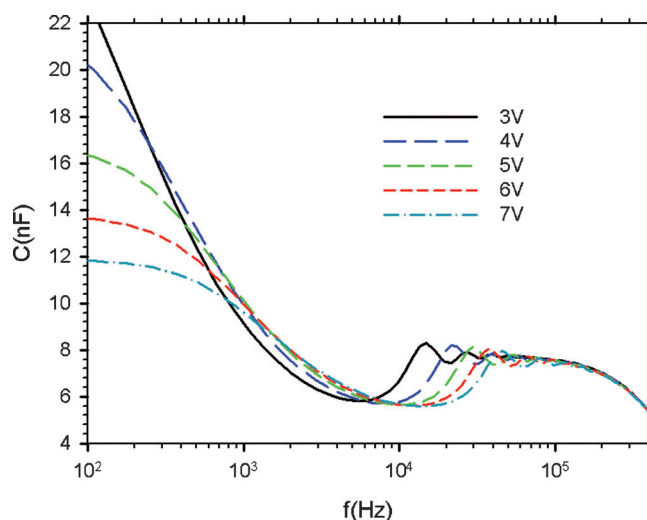


Figure 11. Model representation of capacitance spectra at voltages ranging from 3 to 7 V.

Representative measurements from a thick film of 2-naphthalen-1-yl-5-phenyl-1,3,4-oxadiazole (α-NPD) by Nguyen et al.^[39] are shown in Figure 12. The trends in the data can be understood based on the multiple-trapping features described above.^[93,95] When more voltage is applied to the device, the capacitance spectra exhibit reduced low-frequency capacitance increase and less trap-limited mobility in accordance with our model. Particularly, the latter characteristic can be observed from the transit-time frequencies at different voltages. When more voltage is applied, the capacitance step-up appears closer to the preceding one. Therefore, less deviation in transit times occurs by increasing the voltage, that is, less trapping action that accounts for mobility reduction is present.

5. Interconnection between Transport Models

In the measurements of the SCLC transport in disordered organic semiconductors, it is often observed that charge-carrier mobility depends on bias voltage. The two continuous models applied for the description of this dependence were described in Section 2. One interpretation assumes that carrier mobility is dependent on the local electric field. However, in the other one, mobility is carrier-density dependent.^[96,97] The latter interpretation is equivalent to the trap-controlled transport composed of a transport level affected by multiple trapping of an exponential density. The application of the IS technique, to this framework to determine mobility parameters [Eq. (1)] demonstrated that the apparent field dependence of mobility can be merely understood in terms of the trap-controlled transport model alone.^[49] The trap-limited mobility effect is responsible for the bias-voltage dependence of mobility. Applying more voltage reduces the trap limita-

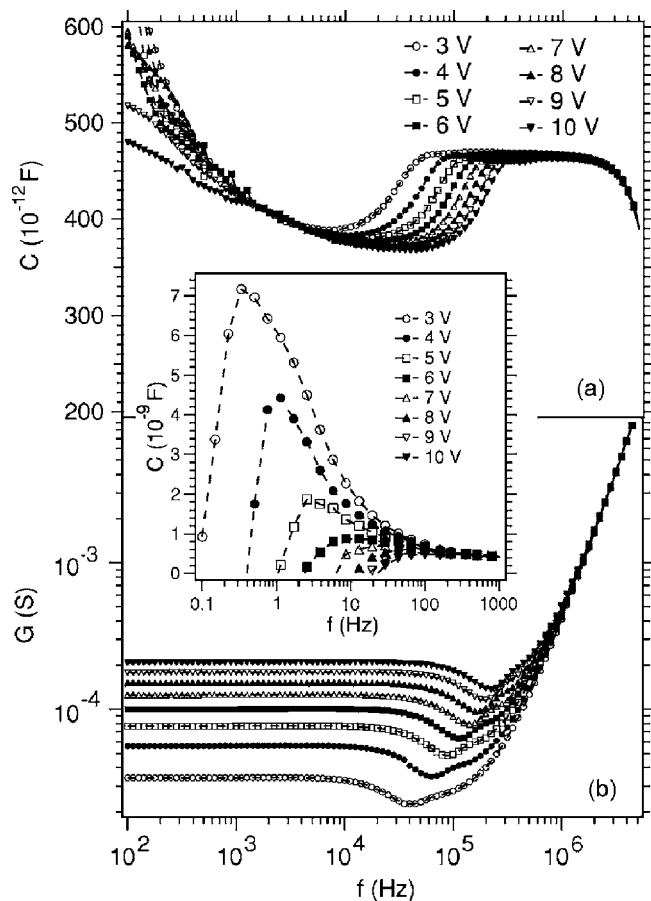


Figure 12. Experimental (a) capacitance, C , and (b) conductance, G , of a hole-only α -NPD device as functions of the modulation frequency, f , for applied dc voltages, V_0 , between 3 and 10 V at room temperature. The inset shows C as a function of f in the low-frequency range (0.1–103 Hz) for the same applied dc voltage values. Reprinted from Ref. [39] with permission from The American Physical Society.

tion of mobility due to less fast traps acting as such in the exponential density (Figure 13). Therefore, the value of mobility becomes higher at increasing voltage.

6. Summary and Outlook

We have provided a unified description of charge transport of injected carriers in disordered organic materials. Trap-controlled transport is understood in terms of SCLC under the trapping–detrapping kinetics of an exponential density of traps in the band gap. Computational simulations reproduce the behavior of experimental capacitance spectra. Low-frequency capacitance increase is attributed to slow traps and mobility dependence on voltage stems from the concept of trap-limited mobility caused by fast traps. Both the depth of the traps and the kinetic coefficients of trapping play a significant role in the measured features. IS therefore appears to be a major tool to char-

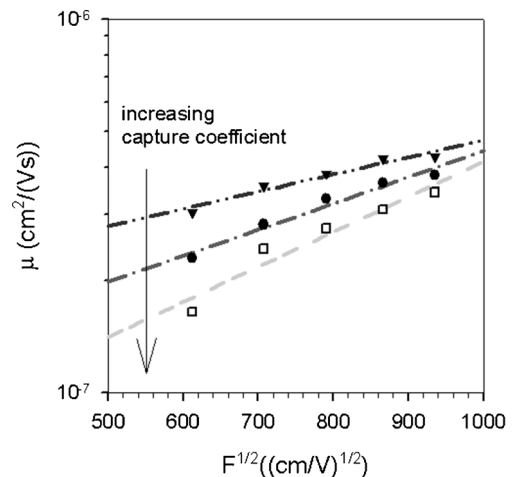


Figure 13. Model representation of mobility versus $F^{1/2}$ by the IS technique for different capture coefficients: $c = 7 \times 10^{-13}$, $c = 4 \times 10^{-12}$, $c = 9 \times 10^{-12} \text{ cm}^3/\text{s}$, from top to bottom. Mobility fittings range from $1.6 \times 10^{-7} \text{ cm}^2/(\text{Vs}) > \mu_0 > 4.8 \times 10^{-8} \text{ cm}^2/(\text{Vs})$ to $1.1 \times 10^{-3} (\text{cm/V})^{1/2} < \gamma < 2.2 \times 10^{-3} (\text{cm/V})^{1/2}$.

acterize both trap distributions and the voltage dependence of mobility in organic layers. Further work is required to provide deconvolution from the measurements of capacitance (IS data) to the intrinsic characterization of the material, that is, the trap distribution and trap kinetics. This research task would allow a full description, as a function of the applied voltage, of the transport and charge accumulation features in organic layers.

Acknowledgements

We thank financial support from the Ministerio de Ciencia e Innovación under project HOPE CSD2007-00007, and Generalitat Valenciana under project PROMETEO/2009/058.

References

- [1] Q. Wang, Y. Ding, Z. Zhang, D. Ma, Y. Cheng, L. Wang, F. Wang, *J. Appl. Phys.* **2009**, *105*, 076101.
- [2] S. Tonzani, *Nature* **2009**, *459*, 312.
- [3] C. W. Tang, S. A. VanSlyke, *Appl. Phys. Lett.* **1987**, *51*, 913.
- [4] J. H. Burroughes, D. D. C. Bradley, A. R. Brown, R. N. Marks, K. MacKay, R. H. Friend, P. L. Burn, A. B. Holmes, *Nature* **1990**, *347*, 539.
- [5] R. H. Friend, R. W. Gymer, A. B. Holmes, J. H. Burroughes, R. N. Marks, C. Taliani, D. D. C. Bradley, D. A. Dos Santos, J. L. Brédas, M. Lögdlund, W. R. Salaneck, *Nature* **1999**, *397*, 121.
- [6] K. Meerholz, *Nature* **2005**, *437*, 327.
- [7] S. Reineke, F. Lindner, G. Schwartz, N. Seidler, K. Walzer, B. Lüssem, K. Leo, *Nature* **2009**, *459*, 234.
- [8] S. R. Forrest, *Nature* **2004**, *428*, 911.

- [9] Y. Shen, A. R. Hosseini, M. H. Wong, G. G. Malliaras, *ChemPhysChem* **2004**, *5*, 16.
- [10] J. C. Scott, G. G. Malliaras, *Chem. Phys. Lett.* **1999**, *299*, 115.
- [11] P. W. M. Blom, M. C. J. M. Vissenberg, *Mater. Sci. Eng.* **2000**, *27*, 53.
- [12] B. K. Crone, P. S. Davids, I. H. Campbell, D. L. Smith, *J. Appl. Phys.* **1998**, *84*, 833.
- [13] P. S. Davids, I. H. Campbell, D. L. Smith, *J. Appl. Phys.* **1997**, *82*, 6319.
- [14] A. L. Alvarez, B. Arredondo, B. Romero, X. Quintana, A. Gutiérrez-Llorente, R. Mallavia, J. M. Otón, *IEEE Trans. Electron Devices* **2008**, *55*, 674.
- [15] J. Bisquert, G. Garcia-Belmonte, J. M. Montero, H. Bolink, *Proc. SPIE* **2006**, *6192*, 619210.
- [16] B. Ruhstaller, S. A. Carter, S. Barth, H. Riel, W. Riess, J. C. Scott, *J. Appl. Phys.* **2001**, *89*, 4575.
- [17] G. Garcia-Belmonte, J. M. Montero, E. M. Barea, J. Bisquert, *J. Appl. Phys.* **2007**, *101*, 114506.
- [18] N. F. Mott, R. W. Gurney, *Electronic Processes in Ionic Crystals*, Oxford University Press, London, **1940**.
- [19] G. T. Wright, *Solid-State Electron.* **1961**, *2*, 165.
- [20] J. Shao, G. T. Wright, *Solid-State Electron.* **1961**, *3*, 291.
- [21] J. Lindmayer, A. Slobodskoy, *Solid-State Electron.* **1963**, *6*, 495.
- [22] P. W. M. Blom, M. J. M. de Jong, M. G. van Munster, *Phys. Rev. B* **1997**, *55*, R656.
- [23] P. W. M. Blom, H. C. F. Martens, J. N. Huiberts, *Synth. Met.* **2001**, *121*, 1621.
- [24] M. M. Mandoc, B. de Boer, P. W. M. Blom, *Phys. Rev. B* **2006**, *73*, 155205.
- [25] M. M. Mandoc, B. de Boer, G. Paasch, P. W. M. Blom, *Phys. Rev. B* **2007**, *75*, 193202.
- [26] S. Shirota, H. Kageyama, *Chem. Rev.* **2007**, *107*, 953.
- [27] M. Jaiswal, R. Menon, *Polym. Int.* **2006**, *55*, 1371.
- [28] D. Poplavskyy, F. So, *J. Appl. Phys.* **2006**, *99*, 033707.
- [29] G. Juška, K. Arlaukas, M. Viliunas, *Phys. Rev. Lett.* **2000**, *84*, 4946.
- [30] F. So, B. Krummacher, D. Poplavskyy, S. A. Choulis, V. Choong, *J. Appl. Phys.* **2007**, *102*, 091101.
- [31] F. Fabregat-Santiago, G. Garcia-Belmonte, I. Mora-Seró, J. Bisquert, *Phys. Chem. Phys.* **2011**, *13*, 9083.
- [32] Q. Wang, S. Ito, M. Grätzel, F. Fabregat-Santiago, I. Mora-Seró, J. Bisquert, T. Bessho, H. Imai, *J. Phys. Chem. B* **2006**, *110*, 25210.
- [33] P. P. Boix, J. Ajuria, I. Etxeberria, R. Pacios, G. Garcia-Belmonte, J. Bisquert, *J. Phys. Chem. Lett.* **2011**, *2*, 409.
- [34] J. Bisquert, G. Garcia-Belmonte, *J. Phys. Chem. Lett.* **2011**, *2*, 1950.
- [35] H. C. F. Martens, H. B. Brom, P. W. M. Blom, *Phys. Rev. B* **1999**, *60*, R8489.
- [36] W. Brütting, S. Berleb, *Phys. Rev. Lett.* **2002**, *89*, 286601.
- [37] H. C. F. Martens, J. N. Huiberts, P. W. M. Blom, *Appl. Phys. Lett.* **2000**, *77*, 1852.
- [38] W. Brütting, H. Riel, T. Beierlein, W. Riess, *J. Appl. Phys.* **2001**, *89*, 1704.
- [39] N. D. Nguyen, M. Schmeits, H. P. Loebel, *Phys. Rev. B* **2007**, *75*, 075307.
- [40] M. Schmeits, *J. Appl. Phys.* **2007**, *101*, 084508.
- [41] B. Ramachandhran, H. G. A. Huizing, R. Coehoorn, *Phys. Rev. B* **2006**, *73*, 233306.
- [42] S. Nowy, W. Ren, A. Elschner, W. Lövenich, W. Brütting, *J. Appl. Phys.* **2010**, *107*, 054501.
- [43] C.-C. Chen, B.-C. Huang, M.-S. Lin, Y.-J. Lu, T.-Y. Cho, C.-H. Chang, K.-C. Tien, S.-H. Liu, T.-H. Ke, C.-C. Wu, *Org. Electron.* **2010**, *11*, 1901.
- [44] D. C. Tripathi, A. K. Tripathi, Y. N. Mohapatra, *Appl. Phys. Lett.* **2011**, *98*, 033303.
- [45] I. Murtaza, I. Qazi, K. S. Karimov, M. H. Sayyad, *Phys. B* **2011**, *406*, 1238.
- [46] T. Okachi, T. Nagase, T. Kobayashi, H. Naito, *Appl. Phys. Lett.* **2009**, *94*, 043301.
- [47] J. M. Montero, J. Bisquert, G. Garcia-Belmonte, E. M. Barea, H. J. Bolink, *Org. Electron.* **2009**, *10*, 305.
- [48] J. M. Montero, J. Bisquert, *J. Appl. Phys.* **2011**, *110*, 043705.
- [49] J. M. Montero, J. Bisquert, *Solid-State Electron.* **2011**, *55*, 1.
- [50] E. Knapp, B. Ruhstaller, *Appl. Phys. Lett.* **2011**, *99*, 093304.
- [51] H. Bässler, *Phys. Status Solidi B* **1993**, *175*, 15.
- [52] P. M. Borsenberger, J. J. Fitzgerald, *J. Phys. Chem.* **1993**, *97*, 4815.
- [53] C. Tanase, P. W. M. Blom, D. M. de Leeuw, E. J. Meijer, *Phys. Status Solidi A* **2004**, *201*, 1236.
- [54] A. B. Walker, A. Kambili, S. J. Martin, *J. Phys.: Condens. Matter* **2002**, *14*, 9825.
- [55] I. H. Campbell, D. L. Smith, C. J. Neef, J. P. Ferraris, *Appl. Phys. Lett.* **1999**, *74*, 2809.
- [56] P. N. Murgatroyd, *J. Phys. D: Appl. Phys.* **1970**, *3*, 151.
- [57] J. M. Montero, J. Bisquert, G. Garcia-Belmonte, H. Bolink, E. M. Barea, *Phys. Status Solidi A* **2007**, *204*, 2402.
- [58] E. M. Barea, G. Garcia-Belmonte, M. Sommer, S. Hüttner, H. Bolink, M. Thelakkat, *Thin Solid Films* **2010**, *518*, 3351.
- [59] H. H. Fong, S. K. So, *J. Appl. Phys.* **2006**, *100*, 094502.
- [60] W. Xu, Khizar-ul-Haq, Y. Bai, X. Y. Jiang, Z. L. Zhang, *Solid State Commun.* **2008**, *146*, 311.
- [61] C. Tanase, E. J. Meijer, P. W. M. Blom, D. M. Leeuw, *Phys. Rev. Lett.* **2003**, *91*, 216601.
- [62] M. C. J. M. Vissenberg, M. Matters, *Phys. Rev. B* **1998**, *57*, 12964.
- [63] V. I. Arkhipov, E. V. Emelianova, G. J. Adriaenssens, *Phys. Rev. B* **2001**, *64*, 125125.
- [64] M. A. Lampert, P. Mark, *Current Injection in Solids*, Academic Press, New York, **1970**.
- [65] A. J. Campbell, D. D. C. Bradley, D. G. Lidzey, *J. Appl. Phys.* **1997**, *82*, 6326.
- [66] G. Paasch, S. Scheinert, *J. Appl. Phys.* **2009**, *106*, 084502.
- [67] H. T. Nicolai, M. M. Mandoc, P. W. M. Blom, *Phys. Rev. B* **2011**, *83*, 195204.
- [68] H. T. Nicolai, A. Hof, J. L. M. Oosthoek, P. W. M. Blom, *Adv. Funct. Mater.* **2011**, *21*, 1505.
- [69] J. Bisquert, *Phys. Rev. B* **2008**, *77*, 235203.
- [70] J. Bisquert, *Phys. Chem. Chem. Phys.* **2008**, *10*, 3175.
- [71] J. Bisquert, *Electrochim. Acta* **2002**, *47*, 2435.
- [72] J. Bisquert, V. S. Vikhrenko, *Electrochim. Acta* **2002**, *47*, 3977.
- [73] J. Shinar, *Organic Light-Emitting Devices: A Survey*, Springer, New York, **2004**.
- [74] I. D. Parker, *J. Appl. Phys.* **1994**, *75*, 1656.
- [75] G. Garcia-Belmonte, J. M. Montero, Y. Ayyad-Limonge, E. M. Barea, J. Bisquert, H. Bolink, *Curr. Appl. Phys.* **2009**, *9*, 414.
- [76] I. Mora-Seró, S. Giménez, T. Moehl, F. Fabregat-Santiago, T. Lana-Villarreal, R. Gómez, J. Bisquert, *Nanotechnology* **2008**, *19*, 424007.
- [77] P. W. M. Blom, M. J. M. Dejong, J. J. M. Vleggaar, *Appl. Phys. Lett.* **1996**, *68*, 3308.
- [78] T. P. Nguyen, *Phys. Status Solidi A* **2008**, *205*, 162.

- [79] A. Rose, *Concepts in Photoconductivity and Allied Problems*, Wiley, New York, **1963**.
- [80] D. Dascalu, *Int. J. Electron.* **1966**, *21*, 183.
- [81] D. Dascalu, *Solid-State Electron.* **1966**, *9*, 1020.
- [82] R. Kassing, *Phys. Status Solidi A* **1975**, *28*, 107.
- [83] R. Kassing, E. Kähler, *Solid State Commun.* **1974**, *15*, 673.
- [84] H. C. F. Martens, H. B. Brom, P. W. M. Blom, J. N. Huiberts, H. F. M. Schoo, *Synth. Met.* **2001**, *121*, 1643.
- [85] S. W. Tsang, S. K. So, J. B. Xu, *J. Appl. Phys.* **2006**, *99*, 013706.
- [86] S. Berleb, W. Brütting, *Phys. Rev. Lett.* **2002**, *89*, 6601.
- [87] A. Pitarch, G. Garcia-Belmonte, J. Bisquert, *J. Appl. Phys.* **2006**, *100*, 084502.
- [88] H. H. P. Gommans, M. Kemerink, G. G. Andersson, R. M. T. Pijper, *Phys. Rev. B* **2004**, *69*, 155216.
- [89] A. Van der Ziel, *Solid State Physical Electronics*, Prentice-Hall, Englewood Cliffs, **1976**.
- [90] K. H. Chan, S. K. So, *J. Photonics Energy* **2011**, *1*, 011112.
- [91] S. Ishihara, H. Hase, T. Okachi, H. Naito, *J. Appl. Phys.* **2011**, *110*, 036104.
- [92] S. Ishihara, H. Hase, T. Okachi, H. Naito, *Org. Electron.* **2011**, *12*, 1364.
- [93] J. V. Li, A. M. Nardes, Z. Liang, S. E. Shaheen, B. A. Gregg, D. H. Levi, *Org. Electron.* **2011**, *12*, 1879.
- [94] S. E. Debebe, W. Mammo, T. Yohannes, F. Tinti, A. Zanelli, N. Camaioni, *Appl. Phys. Lett.* **2010**, *96*, 082109.
- [95] T. Okachi, T. Nagase, T. Kobayashi, H. Naito, *Jpn. J. Appl. Phys.* **2008**, *47*, 8965.
- [96] V. Kumar, S. C. Jain, A. K. Kapoor, W. Geens, T. Aernauts, J. Poortmans, R. Mertens, *J. Appl. Phys.* **2002**, *92*, 7325.
- [97] R. Coehoorn, W. F. Pasveer, P. A. Bobbert, M. A. J. Michels, *Phys. Rev. B* **2005**, *72*, 155206.

Received: September 19, 2011

Accepted: January 25, 2012

Published online: ■ ■ ■, 0000